第 47 卷 第 12 期
2020 年 12 月

湖南大学学报（自然科学版）
Journal of Hunan University (Natural Sciences)

Vol. 47. No. 12.
Dec. 2020

Rough-Sea-Horizon-Line Detection using a Novel Color Clustering and Least Squares Regression Method

Muhammad Umair[1], Manzoor Ahmed Hashmani[1], Horio Keiichi[2]

[1] High-Performance Cloud Computing Center (HPC3), Department of Computer and Information Sciences, Universiti Teknologi PETRONAS, Seri Iskandar, Malaysia

[2] Graduate School of Life Science and Systems Engineering, Kyushu Institute of Technology, Fukuoka, Japan

Abstract: Sea horizon line (SHL) detection is the first step in maritime image processing. It is aimed at object detection, navigation of autonomous aerial and sea surface vehicles, and distance estimation. Many methods have been proposed to detect SHL, however, their focus remains on SHL detection in calm sea conditions. For this reason, this study is designed to fill this gap and investigate an efficient method to detect a sea horizon line under rough sea conditions. A novel color clustering and least-squares regression-based method is proposed to solve the issue. Minimizing computational cost, our method identifies the candidate region of interest (CROI) from grayscale image ROIs by analyzing the modality of its pixel intensity histogram. It then applies *k*-mean clustering to highlight potential sea-sky regions. The regional boundary pixel coordinates are used to construct a horizon line by applying the least-squares regression method. The results of the proposed method were compared to the Canny Edge and Hough Transform (CEHT) method. The gale state sea images were used to test the efficiency of both methods, correctly detecting the starting and ending coordinates of a horizon line and its slope. The results highlight the superiority of the proposed method over the CEHT method. On average, the proposed method identified the horizon line within one degree of error as opposed to CEHT method with the average of five degrees. In half of the images, the error in detecting the horizon starting and ending coordinates for the proposed method was within five or fewer pixels. The overall results show the superiority of the proposed method over the CEHT method in rough sea conditions. The novelty of this study is two-fold. Firstly, it is a pioneering study that proposes a novel method to detect SHL under rough sea conditions. Secondly, the proposed method yielded superior SHL detection results compared to its peers.

Keywords: Sea Horizon Line Detection, Rough Sea Conditions, Candidate Region of Interest, Color Clustering, Least Squares Regression.

一种使用新的颜色聚类和最小二乘回归方法的海平面视线检测

摘要：海平面线（SHL）检测是海上图像处理的第一步。它的目标是物体检测，自动驾驶的空中和海面车辆的导航以及距离估计。已经提出了许多检测 SHL 的方法，然而，它们的重点仍然是在平静海况下的 SHL 检测。因此，本研究旨在填补这一空白，并研究一种在恶劣海况下检测海平面线的有效方法。提出了一种新的基于颜色聚类和最小二乘回归的方法来解决该问题。通过最小化计算成本，我们的方法通过分析像素强度直方图的模态，从灰度图像投资回报率中识别出感兴趣的候选区域（投资回报率）。然后，它应用 k 均值聚类来突出潜在的海天区域。通过应用最小二乘回归方法，区域边界像素坐标用于构建视线。将该方法的结果与坎尼边缘和霍夫变换（中国电子科技大学）方法进行了比较。大风州海洋图像用于测试这两种方法的效率，正确检测

Received (date): September 30, 2020

About the authors: Muhammad Umair, Manzoor Ahmed Hashmani, High-Performance Cloud Computing Center (HPC3), Department of Computer and Information Sciences, Universiti Teknologi PETRONAS, Seri Iskandar, Malaysia; Horio Keiichi, Graduate School of Life Science and Systems Engineering, Kyushu Institute of Technology, Fukuoka, Japan

Corresponding author Muhammad Umair, muhammad_17008606@utp.edu.my , m-umair@outlook.com

地平线的起点和终点及其坡度。结果突出了所提出的方法优于中国电子科技大学方法的优越性。平均而言，与中国电子科技大学方法（平均 5 度）相比，所提出的方法可以将误差范围确定在 1 个误差范围内。在一半的图像中，为所提出的方法检测水平起点和终点的误差在五个或更少的像素以内。总体结果表明，该方法在波涛汹涌的海面条件下优于中国电子科技大学方法。这项研究的新颖性是双重的。首先，这是一项开创性研究，提出了一种在恶劣海况下检测 SHL 的新方法。其次，与同类方法相比，该方法产生了更好的 SHL 检测结果.

关键词：海平面线检测，恶劣海况，候选候选区域，颜色聚类，最小二乘回归

1. Introduction

A sea horizon line (SHL) is a low-level geometric feature in a maritime image that bifurcates the sky and sea regions. By doing so, an area under investigation is isolated, which consequently reduces the computation cost associated with any further computer vision or machine learning task. For such reasons, horizon line detection is usually the first step before addressing issues such as object detection and tracking [1], navigation and collision avoidance of autonomous aerial vehicles [2], [3], steering sea surface vehicles [4], and distance estimation for ships [5].

Under ideal weather conditions, and in an uncluttered maritime scene, an SHL is easily identifiable as the longest and most prominent linear feature. However, in rough sea state scenarios, the presence of high amplitude waves, foam, and water spray may obscure the sea horizon line. In this case, SHL may not be the longest and prominent linear feature in the scene. Identification of SHL in such a situation becomes an interesting and challenging problem in the domain of computer vision. Many sea horizon line detection methods have been proposed in literature. The predominant methods can be divided into three major categories, i.e., projection-based, statistical-analysis-based, and hybrid methods.

The most commonly used method is projection-based. The method assumes that the horizon line is the most noticeable linear feature in a maritime image. Thus, it attempts to find the prominent linear features by applying edge detection and linear feature transform methods [6], [7]. Solutions developed using the projection-based method can be implemented either with 1D or 2D edge detection [4]. They can then apply suitable line detection algorithms such as the least-squares regression method, Hough Transform or Radon Transform, to finally identify the horizon line. However, the presence of other robust linear features induced by wake, water surface color, and floating vegetation may increase the possibility of identifying a false linear feature as a candidate horizon line. Additionally, in rough sea conditions, the horizon line may not be the most prominent linear feature; hence the method may fail in such situations. Moreover, line detection algorithms' high computational complexity is a bottle-neck for projection-based methods [4].

As an alternative, statistical methods have been applied to detect terrestrial/sea horizon line. This approach assumes that the intensity distribution of the sea and sky region is statistically separable, and an intensity variation is present along the horizon. Based on RGB pixel grouping into the sky and sea region, a horizon line, in this case, will have a minimum variance from distinct means of sky and sea regions [6], [7]. However, in rough sea state conditions, as depicted in Fig. 1, grouping the sea or sky regions based on RGB values of pixels becomes challenging due to foam and water spray, which seamlessly blends in with the background.

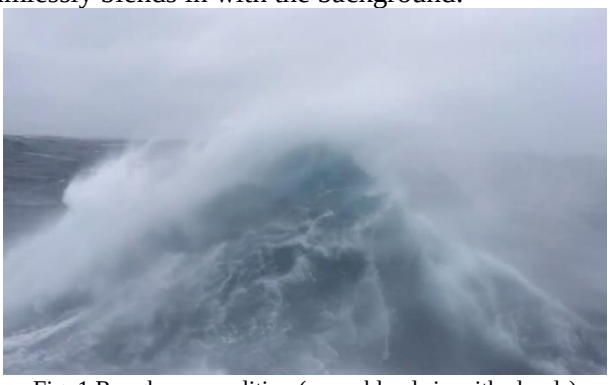

Fig. 1 Rough sea condition (spray blends in with clouds)

The third most commonly used method is based on the hybrid configuration that couples two or more methods to enhance the proposed solution's generalization ability. For example, machine learning methods have been conjugated with edge detection and other techniques to identify the horizon line. An approach based on YCrCb color-based pixel-level binary classification using Support Vector Machine (SVM) and then applying the Hough Transform to the segmented

image to find the horizon line is one example of a hybrid horizon detection method [3]. A similar method applies SVM to classify potential horizon line edges obtained by the Canny Edge detection. It then applies dynamic programming to identify the horizon line [10]. An extension of this method is segmenting each pixel of an edge map into a horizon and non-horizon semantic category and then applying Convolutional Neural Networks (CNN) to identify the edge pixels belonging to the potential sea horizon line [11]. However, these approaches' dependency on the edge map makes them vulnerable to degraded performance under rough sea conditions, where linear features are hard to detect.

The rough sea conditions exhibit challenges such as smooth color intensity change across the sea-sky region, and occlusion of the horizon line by high amplitude waves, spray, and foam. Due to these conditions, robust linear features are mostly absent in the scene, affecting the performance of a projection-based horizon line detection method. Moreover, any hybrid method which is based on an edge map is also subject to degraded performance. Similarly, statistical analysis near the horizon may fail due to smooth color intensity change.

In this paper, we address the issue of detecting the horizon line under rough sea conditions. In such a scenario, we have assumed that the sea horizon line is generally not continuous, and as seen in Fig. 1, it may be obscured by waves, spray, and foam in some regions. Thus, finding the candidate region in which the horizon line is noticeable becomes an essential step in our methodology. Once that candidate region is identified, a partial or full reference of the horizon line can be detected. For this purpose, a binary color clustering technique can be applied. This will segregate the potential sea-sky regions and consequently provides boundary values of the regions. Theoretically, these values can construct a line equation, which subsequently can draw a candidate horizon line. For performance evaluation, our proposed method's results are compared to the Canny Edge and Hough Transform (CEHT) based method. To the best of our knowledge, detecting the horizon line in rough sea conditions is yet to be addressed, and this study is the first step towards solving this issue.

The rest of the paper is divided into the following sections. Section1 discusses our proposed methodology in detail. The data set, ground truth marking, and computational environment are discussed in section 2. Later, section 3 gives details on our proposed and CEHT based experiment and their parameters. Section 4 describes the method used for comparing the results of two experiments. In section 5, we have discussed the results, and subsequently, the conclusion and future directions are given in section 6. Finally, section 7 presents acknowledgment.

2. Research Methodology

Our proposed rough sea horizon line detection (RSHLD) methodology is presented in Fig. 2. It can be divided into four stages. The following subsection explains each stage in detail.

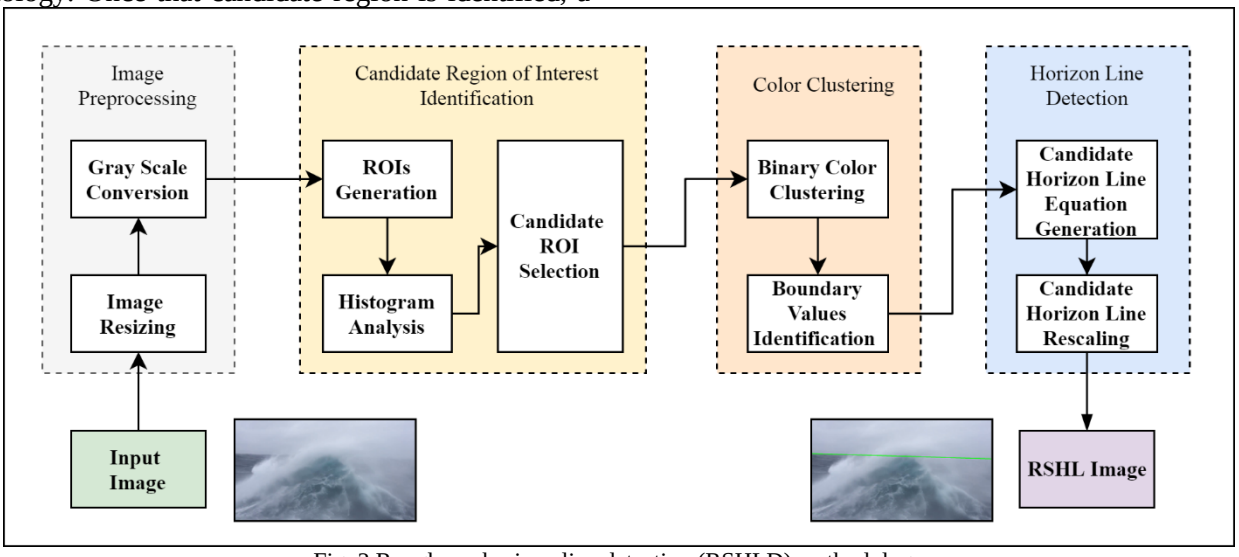

Fig. 2 Rough sea horizon line detection (RSHLD) methodology

2.1. Horizon Line Detection in Rough Sea Conditions

2.1.1. Image Preprocessing

In the first stage, the input image is resized to 50% of its original size while maintaining the aspect ratio. In their literature review, Hashmani et al. [8] reported, from multiple studies, that identifying the sea horizon line in a

color image can increase the computational cost of the method; thus, the resized image is then converted into a grayscale image. This minimizes the computational cost while maintaining the quality of the image at almost at the same level as a color image [8].

2.1.2. Candidate Region of Interest Identification

The identification of a candidate region of interest (CROI) can significantly reduce the computational cost of the method as, now, the region under investigation is smaller than the original image. Thus, in the second stage, the resized grayscale image is horizontally divided into *N* regions of interest (ROIs). Here, the approach adopted by Jeong et al. [9] is considered and 50% overlapping ROIs are generated. The starting and ending pixels for ROIs are computed using equations (1) and (2).

$$ROI_s(n) = \begin{cases} 0, & n = 1 \\ ROI_e(n-1) - HS, & n > 1 \end{cases} \quad (1)$$

$$ROI_e(n) = \begin{cases} FS, & n = 1 \\ ROI_s(n) + FP, & n > 1 \end{cases} \quad (2)$$

Here, $ROI_s(n)$ is the starting pixel and $ROI_e(n)$ is the ending pixel of N^{th} region of interest. FS is the full step size, calculated by dividing the image height by 5 and HS is half step size, calculated by dividing FS by 2. Using this scheme, a total of nine ROIs can be generated for an image.

In rough sea conditions, the sky region generally exhibits a nearly uniform color distribution. Based on this observation, a CROI identification method is proposed. This method uses a gray image pixel intensity histogram to analyze the distribution of pixels in a given ROI. In the case of the presence of only the sky region, a unimodal histogram is generated. However, once the sea region is also present in the ROI, a bimodal distribution is presented in the histogram. This modality change can isolate the ROI in which both sky and sea regions are present. This isolated ROI is considered our CROI.

In the third stage, a binary *k*-means color clustering is applied to the CROI to highlight sky and sea regions. For this purpose, the maximum number of iterations is set to 100, and the desired accuracy is 0.2. The iteration is stopped when either of the criteria mentioned above is met. The initial cluster center is randomly picked. Since the CROI is a small portion of a resized grayscale image, the computational cost of *the k*-means clustering is minimal. The creation of two-color clusters provides the pixel level information for two distinct regions. The change of pixel color in the vertical direction indicates the boundary of the regions. Based on this information, all such boundary pixel coordinates are identified.

The sea horizon line in rough sea conditions generally does not exhibit linear characteristics. In the fourth and the final stage, the coordinates of boundary pixels are used to construct the candidate sea horizon line equation by applying the least-squares regression method. The steps to generate the equation are presented in equations (3-7).

$$\bar{X} = \frac{\sum_{i=1}^{n} x_i}{n} \quad (3)$$

$$\bar{Y} = \frac{\sum_{i=1}^{n} y_i}{n} \quad (4)$$

$$m = \frac{\sum_{i=1}^{n} (x_i - \bar{X})(y_i - \overline{Y})}{\sum_{i=1}^{n} (x_i - \bar{X})^2} \quad (5)$$

$$b = \bar{Y} - m\bar{X} \quad (6)$$

$$y = mx + b \quad (7)$$

Here $\bar{X}$ and $\bar{Y}$ are the means of x and y coordinate values of boundary pixels, m is the slope, and b is the y-intercept. At this point, the candidate horizon line is generated by using equation (7) for solving it for the value of x. For mapping the horizon line on the original image, its coordinates are re-calculated by upscaling it with the image resize factor. The methodology at this stage generates the original image with the candidate sea horizon line marked on it. The algorithm of our proposed methodology is presented below.

Algorithm 1: Rough Sea Horizon Line Detection

Input	:	rough sea image, **RS**
Output	:	rough sea horizon line, **RSHL**
Step 1	:	$\mathbf{S_D}$ ← downsize **RS** to 50%
Step 2	:	$\mathbf{GS_D}$ ← convert $\mathbf{S_D}$ to grayscale
Step 3	:	∑**ROI**← generate a region of interest for $\mathbf{GS_D}$
Step 4	:	**CROI** ← identify a candidate region of interest from ∑**ROI**
Step 5	:	apply binary k-mean clustering on **CROI** **C1** ← color cluster 1 **C2** ← color cluster 2
Step 6	:	$\sum \mathbf{P_B}$ ← identify color cluster**C1, C2** boundary pixels
Step 7	:	$\mathbf{HL_{EQU}}$ ← apply the least-squares regression method to generate a line equation using $\sum \mathbf{P_B}$
Step 8	:	**HL** ← solve $\mathbf{HL_{EQU}}$ for x coordinate values of $\mathbf{S_D}$
Step 9	:	**RSHL** ← upsize the **HL** by 50%
Step 10	:	generate rough sea horizon line **RSHL** image

2.2. Experimental Setup

As discussed earlier, the proposed method aims to detect the horizon line in rough sea conditions. Thus, we have considered a Beaufort wind scale level 8 sea conditions for this problem. The Beaufort wind scale is an empirical scale introduced by Admiral Beaufort to report the sea conditions corresponding to wind speed. It has been recommended for international use since 1874 [10].

2.2.1. Data Set

Since none of the available maritime image data sets cover rough sea state conditions [8], we have selected a

public video source for creation of the required data set [11]. The video consists of 3,670 frames at a resolution of 1280 x 720 pixels. It was recorded while transiting from Seattle to San Diego, USA, from the main deck of the starboard side of a scientific research vessel. During the transit, a Beaufort 10 scale sea state was reported. However, by comparing a sample frame from the video with a standard reference [12], the actual Beaufort state was found to be closer to state 8. At this state, the wind speed was between 32 to 37 *kn* per hour and the Beaufort scale description of this state is "gale" [10]. For the interest of the reader, the comparative images are presented in Fig. 3.

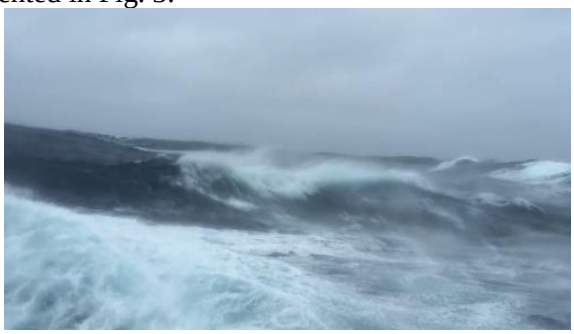

(a) Actual video frame

(b) Beaufort scale 7 sea state reference

(c) Beaufort scale 8 sea state reference

Fig. 3 Manual sea state identification using standard reference images

From the source video, 3 frames per second were extracted and saved in portable network graphics (PNG) format. The resolution of the frames was 1280 x 720 pixels with a 24-bit depth. The frames were named in a sequence starting from 0 with a step size of 10 (i.e., frame 0, frame 10, frame 20). In total, 367 frames were extracted. These frames cover different situational categories including a visible horizon line, partially occluded horizon due to high-amplitude waves, water spray, foam, irregular horizon line, partial and full blur images, thus making it a challenging data set. Some sample images from the generated data set are presented in Fig. 4.

(a) Visible horizon

(b) Partially visible horizon

(c) Water spray

(d) Foam

(e) Irregular horizon

(f) Partial blur

Fig. 4 Different conditions of the sea present in the data set

2.3. Ground Truth Marking

Ground truth marking is essential for evaluating the performance of a method. For this reason, the presence of the horizon line in all 367 images was manually observed. It was found that in 8 images, the horizon line was not visible due to dominating water spray. Thus 359 images were finally selected and manually marked by identifying the starting and ending points of the visible horizon line. In all images, the x-axis coordinates were 0 and 1279; however, the values for y-axis coordinates changed from frame to frame. The ground truth horizon lines (GTHLs) were then drawn using those points. In the later stage, for all GTHLs, slope angles (S_{angle}) were calculated in degrees. These values were later used to gauge the efficiency of the results generated by our experiment. Table 1 presents the generated data set statistics.

Table 1 Data set statistics

(a) Frame Statistics			
Total Number of Frames	359		
Frame Resolution	1280 x 720 pixels		
Bit Depth	24		
(b) Ground Truth Statistics			
	Starting Pixel (x_0, y_0)	Ending Pixel (x_{n-1}, y_{n-1})	S_{angle}(Degree)
Minimum	(0,130)	(1279,131)	-8.62
Maximum	(0,488)	(1279,427)	9.19
Mean of y	303	291	-
Deviation of y	64	65	-

2.4. Computational Environment

Python has been widely used in image processing applications. Its ease of use makes it an ideal choice for the implementation of our proposed methodology. For image processing, the OpenCV library was used. The code was written on Jupyter Notebook and executed on an Intel i5-4200U processor running a 64-bit operating system.

3. Experiment

For the comparative performance analysis, the experiment is divided into two parts. The first part is based on our proposed methodology, and the second partis conducted using the CEHT based horizon line detection method. All 359 images were resized to 50% of their original dimensions for both experiments while maintaining their aspect ratio. Since from this point onwards, the experiments followed two different flows. Thus, they are separately discussed in the following two sub-sections.

3.1 Proposed Rough Sea Horizon Line Detection (RSHLD) Algorithm based Experiment

The resized images are converted into grayscale, and for every image, the coordinated of ROIs are identified using equations (1) and (2). The results of ROI generation are presented in Fig. 5.

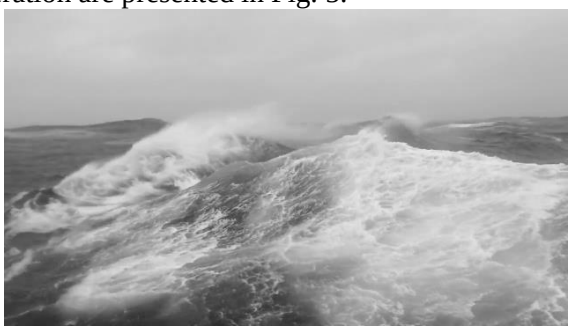

(a) Resized gray scale image

(b) ROI 1

(c) ROI 2

(d) ROI 3

(e) ROI 4

(f) ROI 5

(g) ROI 6

(h) ROI 7

(i) ROI 8

(j) ROI 9

Fig. 5 Region of interest generation

Once the ROIs are generated, the proposed histogram modality analysis is performed, and a candidate ROI is identified. The results of CROI identification are presented in Fig. 6.

A two centers *k*-means clustering is then applied to CROI to group the pixels which belong to sea and sky regions. Later, the identified color clusters' values are used to identify the boundary between the two clusters. For this purpose, a pixel-by-pixel vertical scan is performed across the x-axis. The coordinates of change in a pixel's color value are marked as boundary values. These boundary values are used to generate the horizon line equation using the least-squares regression method. Once the horizon line equation is formed, a horizon line is constructed on the original image by solving it for the value of x and resizing it as per the original image's dimensions. Fig. 7 exhibits the outcomes of each step discussed above.

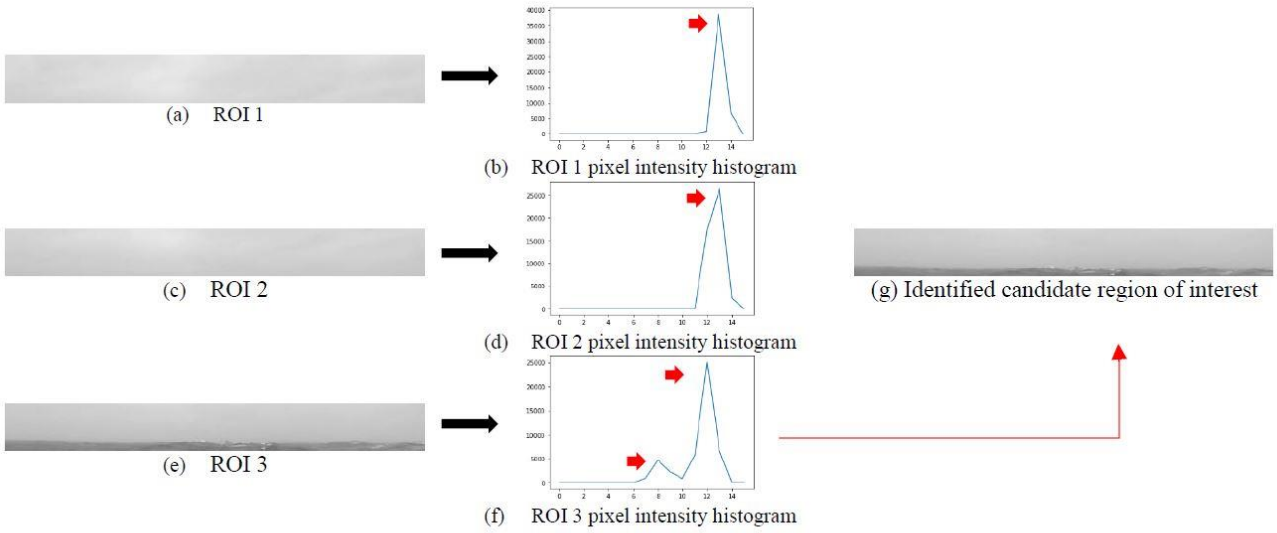

Figure 6. Histogram modality analysis for candidate region of interest identification

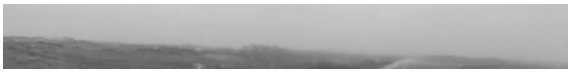

(a) Candidate region of interest

(b) Binary color clustering

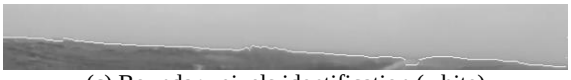

(c) Boundary pixels identification (white)

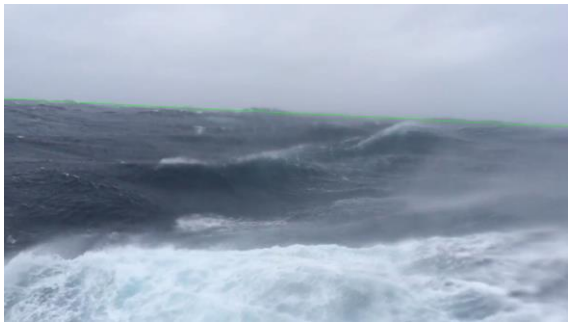

(d) Detected horizon line (green)

Fig. 7 Rough sea horizon line detection using the proposed RSHLD method

3.2 Canny Edge and Hough Transform (CEHT) based Horizon Line Detection Experiment

Canny Edge and Hough Transform is a well-known method for horizon line detection [9],[13],[14]. For this

reason, it is chosen for the performance analysis of the proposed method. To implement this method, a median filter of size 5x5 is applied to the resized image. This filter effectively removes the noise from the image while preserving the edge information [15]. The resultant image is then converted into a grayscale image, and ROIs are generated using equations (1) and (2). The proposed histogram modality analysis is then applied to identify CROI. The Canny Edge operator is then applied to CROI. The lower and upper thresholds for the Canny Edge operator are calculated using proposed equations (8-10).

$$PA_{img} = \frac{\widetilde{P_{img}} + \mu(P_{img})}{2} \quad (8)$$

$$LT = \max(0, (1 - C) * PA_{img}) \quad (9)$$

$$UT = \min(255, (1 + C) * PA_{img}) \quad (10)$$

Here, PA_{img} is the average of median and mean values of grayscale image pixels P_{img}, C is a control variable from 0 to 1. LT is the lower, and UT is the upper threshold for the Canny edge operator. Once the edges are detected, probabilistic Hough Transform is applied to the edge map, and the longest line found is selected as the candidate horizon line.

Since the Hough Transform returns the line's starting and ending points, a line equation is derived from this information. This line equation is finally used to draw the horizon line on the original image by adjusting it as per new coordinates. The outcomes of this experiment are presented in Fig. 8.

(a) Candidate region of interest

(b) Canny edge detection

(c) Hough transform line (white)

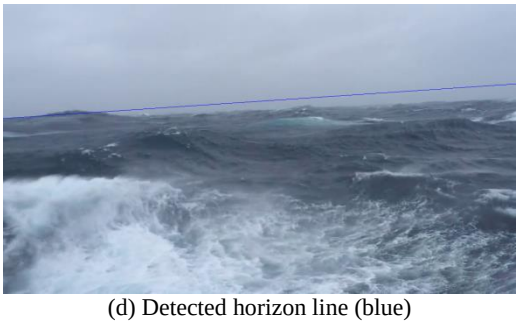

(d) Detected horizon line (blue)

Fig. 8. Rough sea horizon line detection using CEHT method

3.3. Comparison Method

The results of two experiments are compared using ground truth horizon line (GTHL) values described in Table 1. Here, two parameters are considered for comparison. The first parameter (i.e., horizon starting and ending coordinates) is used to compare the RSHLD and CEHT method's pixel-level accuracy. The second parameter (i.e., horizon line slope) is used to compare the accuracy of finding the horizon line's correct angle by both methods.

4. Results and Discussion

Two experiments for rough sea horizon line detection are designed, performed, and their results are generated. In this section, we discuss those results in detail.

The method of finding a candidate region of interest requires that an image is first divided into N equal size of regions of interest. We find that generating a 50% overlapping ROI helps minimize the occurrence of the sea-sky region at the very bottom or top section of an ROI and helps capture different sea-sky regions. Fig. 5 (d) is one such example. This overlapping technique is found to be effectively capturing the significant presence of both regions in 89% of cases. However, there are few examples, such as Fig. 9, in which a small region of the sea is visible at the boundary of ROI. To some extent, we find that few such ROIs affected the performance of significant CROI identification in a later stage.

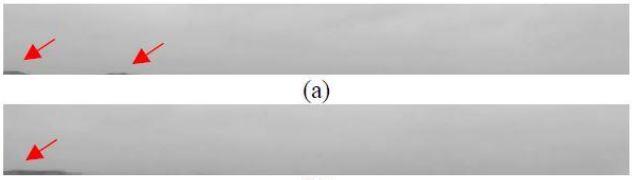

(a)

(b)

Figure 9. Sea region (red arrows) at the boundary of ROI

As mentioned in Table 2, the proposed CROI identification method (as depicted in Fig. 6) shows promising results, and out of 359 frames, CROI was identified in 345 frames. A visual analysis of these CROIs is conducted, and it is found that out of 345 CROIs, 337 CROIs successfully captured significant sea-sky regions. This shows an overall efficiency of 94% in detecting correct CROIs. It is found that ROI in which a significant sea-sky region is not present, the dominant cloud region caused a bimodal nature of its pixel intensity histogram; thus, the method identified the wrong CROI. One such example is presented in Fig. 10.

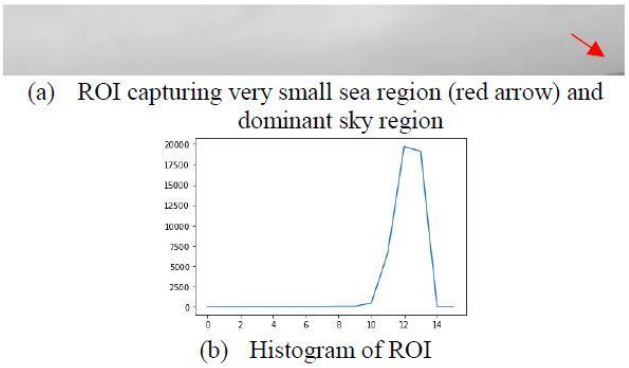

(a) ROI capturing very small sea region (red arrow) and dominant sky region

(b) Histogram of ROI

Figure 10. Wrong CROI identification

Table 2: CROI and *k*-mean color clustering results

Total Frames	Selected Frames	CROI Identified	Correct CROI Identified	Binary Color Clusters Identified from CROI	Correct Binary Color Clusters Identified
367	359	345	337	345	310
	Accuracy	96%	94%	100%	86%

Hence, it is recommended that the histogram of the current plus 1 ROI may also be examined to select the correct CROI.

The binary *k*-mean clustering is used to assign the pixels to two groups, i.e., sea and sky. Since it is applied to CROI, a small portion of a downsized image, computation cost remains low. As presented in Table 2, all 345 CROIs were processed, and it is found that 86% of identified clusters correctly bifurcated the two regions. The presence of a small sea-region and blur caused by the water spray contributed to the regions' incorrect color clustering.

The coordinates of boundary pixels of two regions are used to construct the candidate horizon line equation by applying the least-squares regression method. As described in Table 3, our proposed method is able to identify lines in 335 frames. However, in 87% of the frames (i.e., 312 frames), the line had all or some GTHL properties. It is found that wrong color clustering was a major factor in the misidentification of the horizon line in the remaining 13% of the frames (i.e., 23 frames). Despite this issue, overall, the mean difference between GTHL's slope angle and the proposed RSHLD horizon lines' slope angle is as low as 1 degree with a standard deviation of 1.3 degrees, which is a satisfactory result given that the CROI and color clustering performance is affected by the complexity of rough sea conditions. The mean error of detecting the correct starting and ending point of the horizon line is 14 and 20 pixels, respectively. It is also encouraging that the proposed method can detect the horizon line in most challenging rough sea conditions as well. Fig. 11 depicts some of these results.

(a) Ground truth (frame 2490)

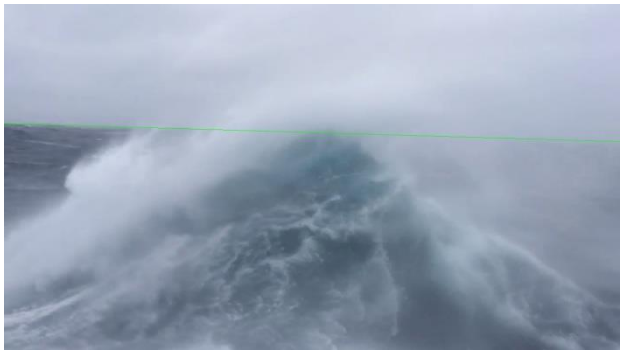

(b) Detected horizon line (frame 2490)

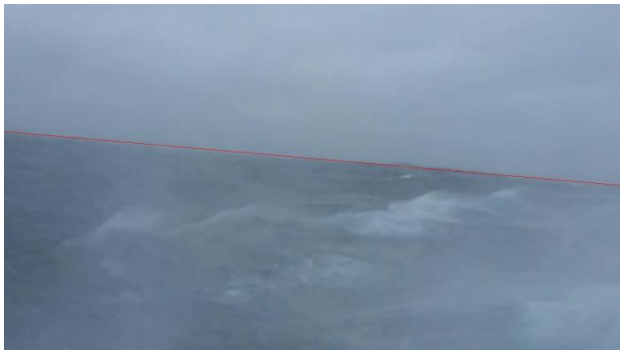

(c) Ground truth (frame 3570)

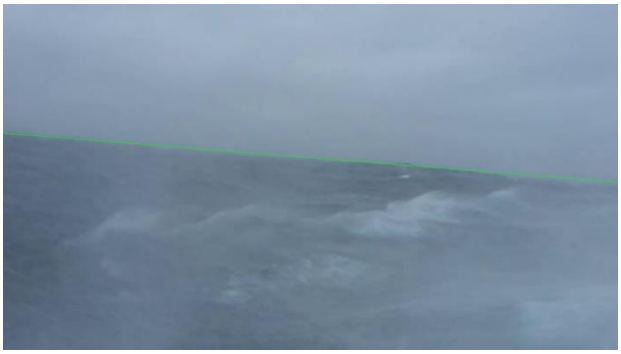

(d) Detected horizon line (frame 3570)

(e) Ground truth (frame 3530)

(f) Detected horizon line (frame 3530)

Fig. 11 Ground truth (a, c, e), and detected horizon line result using RSHLD method (b, d, f)

The results of our proposed method are compared with the CEHT-based method. It is observed that in rough sea conditions, edge-based line detection is generally less effective in determining the sea horizon line. As presented in Table 3, out of 359 frames, the Canny operator is able to detect edges in 124 frames which is a 34.5% success rate. From these 124 frames, most horizon lines generated by the Hough Transform did not align with the GTHLs.

Table 3 Performance statistics for RSHLD and CEHT based methods in rough sea conditions

	Line Identified (Frames)	**Mean y_0 Error (Pixels)**	**Mean y_{n-1} Error (Pixels)**	**Mean Horizon Line Angle Error (Degree)**	**Horizon Line Angle Standard Deviation (Degree)**
RSHLD Method	335	14	20	1.0	1.3
CEHT Method	124	51	70	5.0	4.9

The difference between the mean slope angle of this method and GTHLs slope angles is 5.0 degrees with a standard deviation of 4.9 degrees. Similarly, the mean error of detecting the correct start and endpoint of the horizon line is 51 and 70 pixels, respectively. This shows the inefficiency of the Canny edge and Hough transform (CEHT) based method in detecting the true horizon line in the sea horizon line. This could be attributed to the absence of strong linear features in rough sea conditions. Fig. 12 represents the comparative results of our proposed and CEHT method.

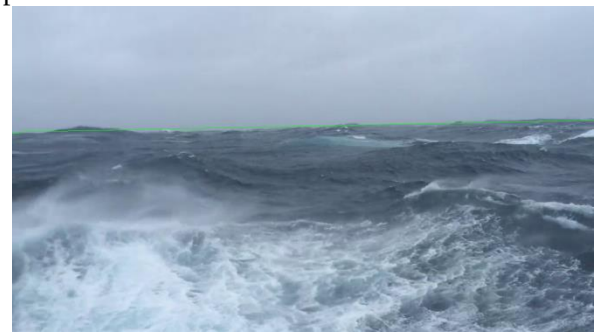

(a)

(b)

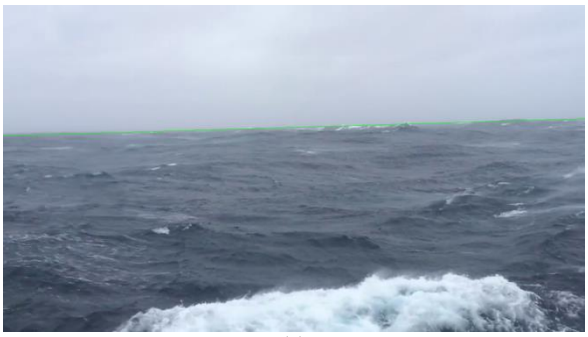

(c)

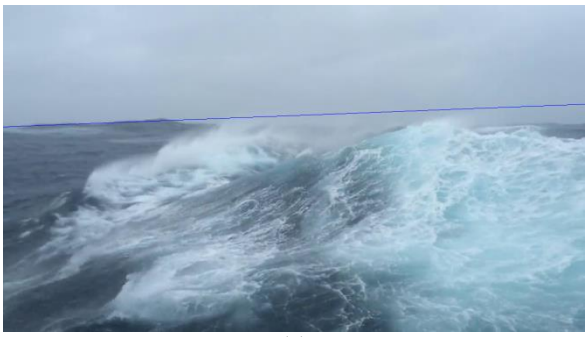

(g)

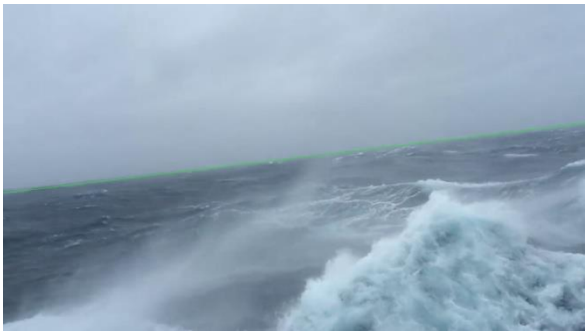

(d)

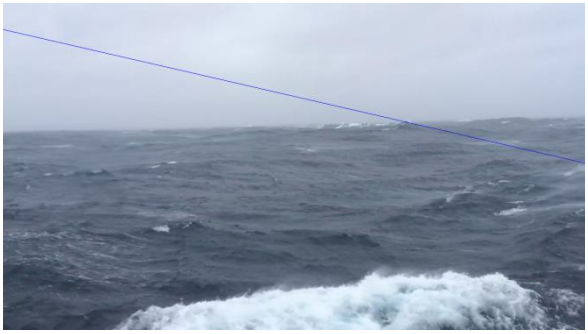

(h)

(e)

(i)

(f)

(j)

Fig. 12 Horizon line detection results of RSHLD (a, b, c, d, e) and CEHT (f, g, h, i, j) methods under different rough sea conditions

5. Conclusions and Future Work

A novel rough-sea-horizon-line detection (RSHLD) method based on binary color clustering and least-squares regression method was proposed, and its results were compared to the CEHT-based horizon line detection method.

Image frames extracted from Beaufort State 8 videos were used to test the efficiency of both methods. A candidate region of the interest identification method based on the modality analysis of a pixel intensity histogram was also tested, identifying the correct candidate region with an accuracy of 94%.

It was found that Canny edge detection was not effective under rough sea conditions. Out of 359 images, it was able to detect edges in only 124 frames. Since Canny edge detection is a precursor to Hough transform line detection, the generated line results were also affected. Compared to ground truth values, the generated results had a mean slope angle error of 5 degrees with a standard deviation of 4.9 degrees. The Canny edge method suffers from a lack of strong linear features in rough sea conditions; hence, it detected the start and endpoints of the horizon line with a mean error of 50 and 70 pixels, respectively.

The proposed method produced better results in rough sea conditions and was able to detect a line in 335 frames. However, there were cases when the identified line was completely unrelated to the ground truth horizon line. This could be attributed to misidentified CROI and subsequent wrong color clusters. Nevertheless, the method generated promising results in complex and rough sea conditions. Overall, an average error of 1 degree with a standard deviation of 1.3 degrees was observed as compared to ground truth values. In half of the cases, the error in finding the correct start and endpoints of the horizon line was five or fewer pixels. In the case of an irregular horizon, partial occlusion, and blur, promising results were generated by the proposed method.

To the best of our knowledge, this is a pioneer study in detecting the horizon line in rough sea conditions, and it has produced promising results. The proposed method could be used for isolating a target region for maritime object detection or as a reference for navigational purposes in rough sea conditions.

Finally, it was observed that the misidentification of CROI and wrong color cluster identification played major roles in detecting a false horizon line. In the future, a more optimized method of selecting CROI could be further investigated. In addition to this, other clustering methods, such as density-based methods, may be further evaluated.

Acknowledgment

This research work is a part of an ongoing research project funded by Yayasan Universiti Teknologi PETRONAS – Fundamental Research Grant (YUTPFRG)- 2019.

References

[1] SHAN X., ZHAO D., PAN M., WANG D. and ZHAO L. Sea-sky line and its nearby ships detection based on the motion attitude of visible light sensors. *Sensors (Switzerland)*, 2019, 19(18): 1–23.

[2] TODOROVIC S. and NECHYBA M.C. A vision system for intelligent mission profiles of micro air vehicles. *IEEE Transactions on Vehicular Technology*., 2004, 53(6): 1713–1725. https://doi.org/10.1109/TVT.2004.834880

[3] MCGEE T. G., SENGUPTA R., and HEDRICK K. Obstacle Detection for Small Autonomous Aircraft Using Sky Segmentation. *Proceedings of the 2005 IEEE International Conference on Robotics and Automation*, Barcelona, Spain, 2005: 4679-4684, https://doi.org/10.1109/ROBOT.2005.1570842.

[4] DEL PIZZO S., GAGLIONE S., ANGRISANO A., SALVI G., and TROISI S. Reliable vessel attitude estimation by wide angle camera. *Measurement: Journal of the International Measurement Confederation*, 2018, 127, (January): 314–324, https://doi.org/10.1016/j.measurement.2018.05.104

[5] GLADSTONE R., MOSHE Y., BAREL A., and SHENHAV E. Distance estimation for marine vehicles using a monocular video camera. *24th European Signal Processing Conference (EUSIPCO)*, Budapest, 2016: 2405-2409, https://doi.org/10.1109/EUSIPCO.2016.7760680.

[6] ETTINGER S.M., NECHYBA M.C., IFJU P.G., and WASZAK M. Vision-Guided Flight Stability and Control for Micro Air Vehicles. *IEEE/RSJ International Conference on Intelligent Robots and Systems*, Lausanne, Switzerland, 2002, 3: 2134-2140, https://doi.org/10.1109/IRDS.2002.1041582.

[7] FEFILATYEV S., GOLDGOF D., SHREVE M., and LEMBKE C. Detection and tracking of ships in open sea with rapidly moving buoy-mounted camera system. *Ocean Engineering*, 2012, 54: 1–12, https://doi.org/10.1016/j.oceaneng.2012.06.028

[8] HASHMANI M. A., UMAIR M., HUSSAIN RIZVI S.S., and REHMAN GILAL A. A Survey on Edge Detection based recent Marine Horizon Line Detection Methods and their Applications. *3rd International Conference on Computing, Mathematics and Engineering Technologies (iCoMET)*, Sukkur, Pakistan, 2020: 1-5, https://doi.org/10.1109/iCoMET48670.2020.9073895.–5.

[9] JEONG C.Y., YANG H.S., and MOON K.D. Fast horizon detection in maritime images using region-of-interest. *International Journal of Distributed Sensor Networks*, 2018, 14(7), https://doi.org/10.1177/1550147718790753

[10] LAING A. K. *et al.*, *Guide to Wave Analysis and Forecasting*. 1998.

[11] STOFFREGEN T. Force 10 on the Beaufort Scale - Balance research ship. 2016. https://www.youtube.com/watch?v=1BXCMoQhnBU.

[12] UNITED STATES NATIONAL WEATHER SERVICE. Sea State Photographs for Determining Wind Speed. in *U.S. Government Posters, Book 59*, 1987.

[13] GERSHIKOV E. Horizon Line Detection in Marine Images: Which Method to Choose? *International Journal on Advances in Intelligent Systems*, 2013, 6(1–2): 79–88.

http://citeseerx.ist.psu.edu/viewdoc/download?doi=10.1.1.682.4145&rep=rep1&type=pdf
[14] PRASAD D.K., RAJAN D., RACHMAWATI L., RAJABALLY E., and QUEK C. MuSCoWERT: multi-scale consistence of weighted edge Radon transform for horizon detection in maritime images. *Journal of the Optical Society of America A*, 2016, 33(12): 2491-2500, https://doi.org/10.1364/JOSAA.33.002491
[15] MARAGOS P., *Morphological Filtering*, 1st ed. Elsevier, 2009.

参考文:

[1] SHAN X., ZHAO D., PAN M., WANG D. 和 ZHAO L. 基于可见光传感器运动姿态的海天线及其附近船舶探测。传感器（瑞士），2019，19（18）：1–23。
[2] TODOROVIC S.和 NECHYBA M.C. 用于微型飞行器智能任务配置文件的视觉系统。 IEEE 车辆技术学报，2004，53（6）：1713-1725。
[3] MCGEE T. G.，SENGUPTA R.和 HEDRICK K. 使用天空分割的小型自主飞机的障碍物检测。 2005 年在西班牙巴塞罗那举行的 2005 年 IEEE 机器人与自动化国际会议国际会议论文集：2005，4：4679-4684。
[4] DEL PIZZO S.，GAGLIONE S.，ANGRISANO A.，SALVI G.和 TROISI S. 通过广角摄像机进行可靠的船只姿态估计。测量：国际测量联合会杂志，2018，127，（一月）：314–324。
[5] GLADSTONE R.，MOSHE Y.，Barel A.和 SHENHAV E. **使用**单目摄像机对海洋车辆进行**距离估**计。**第** 24 **届欧洲信号**处理会议（EUSIPCO），**布达佩斯**，）：2405-2409。
[6] ETTINGER S.M.， NECHYBA M.C.， IFJU P.G. 和 WASZAK M. **微型航空器的**视觉引导飞行稳定性和控制。IEEE/RSJ **国**际智能机器人和系统国际会议，**瑞士洛桑**，2003, 17（7）：617-640。
[7] FEFILATYEV S.， GOLDGOF D.， SHREVE M. 和 LEMBKEC。使用快速移动的安装在浮标上的摄像头系统在公海中检测和跟踪船舶。**海洋工程**，2012，54：1-12。
[8] HASHMANI M. A.，UMAIR M.，HUSSAIN RIZVI S.S. 和 REHMAN GILALA。基于边缘检测的调查，**基于最近的海洋**视线检测方法及其应用。 2020 基于边缘检测的调查，基于最近的海洋视线检测方法及其应用。第三届计算，数学和工程技术国际会议（iCoMET），巴基斯坦苏库尔, 1-5。
[9] JEONG C.Y.，YANG H.S.和 MOON K.D. **使用感**兴趣区域快速检测海上图像中的地平线。**国**际分布式传感器网络杂志，2018，14（7）https://doi.org/10.1177/1550147718790753
[10] LAING A. K. 等人，《波浪分析和预报指南》。 1998.
[11] STOFFREGEN T. **在** Beaufort **磅秤上使用** 10 **号力量-平衡研究船**。2016。可从 https://www.youtube.com/watch?v=1BXCMoQhnBU 获得。[访问：2020 年 6 月 20 日]。
[12] 美国国家气象局。确定风速的海况照片。**在我**们中。**政府海**报，59，1987。
[13] GERSHIKOV E. **海洋影像中的地平**线检测：选择哪种方法？**国**际智能系统进展杂志，2013，6（1-2）：79-88。
[14] PRASAD D.K.， RAJAN D.， RACHMAWATI L.， RAJABALLY E.和 QUEK C. MuSCoWERT：加权边缘 Radon 变换的多尺度一致性，用于海上图像中的地平线检测。美国光学学会杂志 A，2016，33（12）：2491。
[15] MARAGOS P.，《形态过滤》，**第一版**。爱思唯尔，2009.